Controlled Multibubble Surface Cavitation

Nicolas Bremond,* Manish Arora, Claus-Dieter Ohl, and Detlef Lohse†

Physics of Fluids, University of Twente, Post Office Box 217, 7500 AE Enschede, The Netherlands

(Received 13 December 2005; published 5 June 2006)

Heterogeneous bubble nucleation at surfaces has been notorious because of its irreproducibility. Here controlled multibubble surface cavitation is achieved by using a hydrophobic surface patterned with microcavities. The expansion of the nuclei in the microcavities is triggered by a fast lowering of the liquid pressure. The procedure allows us to control and fix the bubble distance within the bubble cluster. We observe a perfect quantitative reproducibility of the cavitation events where the inner bubbles in the two-dimensional cluster are shielded by the outer ones, reflected by their later expansion and their delayed collapse. Apart from the final bubble collapse phase (when jetting flows directed towards the cluster's center develop), the bubble dynamics can be quantitatively described by an extended Rayleigh-Plesset equation, taking pressure modification through the surrounding bubbles into account.

DOI: 10.1103/PhysRevLett.96.224501 PACS numbers: 47.55.dp, 47.55.dd

Cavitation is difficult to control and to quantitatively reproduce. This holds, in particular, for cavitation at surfaces (heterogeneous nucleation), as details such as the wall roughness and its local hydrophobicity strongly matter. As water is normally contaminated with floating microparticles, heterogeneous nucleation is considered to be more relevant than homogeneous cavitation.

For a single isolated bubble in the bulk the radial dynamics in an acoustic field is meanwhile well understood [1–3], also thanks to the discovery and understanding of single bubble sonoluminescence; see, e.g., [4]. This holds much less for interacting bubbles. Though there had been considerable progress on the numerical and theoretical side [5–10], experiments have remained difficult, mainly because radial and translational dynamics of the bubbles are coupled to each other [11–13].

In this Letter we combine surface cavitation and cloud cavitation by heterogeneous nucleation of bubbles on a patterned hydrophobic surface, in which the bubble nuclei are predetermined by micrometer cavities. If the surface is exposed to water, air is entrapped in these cavities, which nucleate hemispherical surface bubbles on pressure reduction. Through the method of micropatterning of the surface we have perfect control on the bubbles' positions and distances, decoupling them from their radial motion. Therefore we can study the interaction of the bubbles in a controlled way, and proceed in the understanding of bubble clusters. The procedure is quantitatively reproducible to such a degree that high-speed movies of the cavitation process can be taken by simply gradually shifting the moment when the picture is taken, relative to the moment of pressure reduction.

The heterogeneous bubble nucleation at a surface and the subsequent cavitation studied here has applications in medicine for breaking kidney stones (lithotripsy) or ultrasound cleaning devices [2], but also unwanted consequences such as cavitation damage at ship propellers [2,14]. The work is also relevant to better understand boiling, where the bubble nucleation at the surfaces is achieved through heating. Finally, the method may help to shed light on the paradox of surface nanobubbles [15,16], which could be visualized by pressure reduction and the resulting cavitation.

The experimental procedure is as follows: The substrates are 3 mm by 5 mm plates diced from a silicon wafer. Cylindrical cavities 15 μm deep with a diameter $D = 4$ μm are etched on the wafer using the deep reactive ion etching technique (Fig. 1). The substrates are finally coated with perfluorodecyltrichlorosilane (FDTS) through vapor deposition leading to an advancing contact angle of water equal to $106° \pm 1°$. These hydrophobic cavities act as gas traps and therefore promote the nucleation of bubbles once the liquid pressure is lowered. The pressure pulse is generated with the help of a piezoelectric transducer (Piezoson 100, Richard Wolf GmbH) made of piezoceramic elements arranged on a portion of a sphere [17].

The pressure pulse device is connected to a rectangular tank containing 1 l of Milli-Q water saturated with gas at

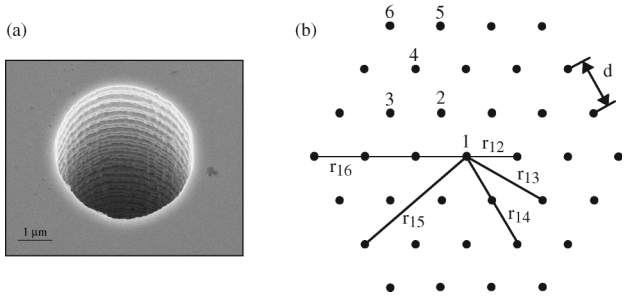

FIG. 1. (a) Electron microscopy image of an individual hydrophobic microcavity (diameter 4 μm) etched on a silicon plate acting as gas trap. (b) Sketch of the spatial distribution of the artificial nuclei set on a hexagonal lattice with a pitch $d = 200$ μm. The nuclei fall into six different classes denoted by the numbers 1 to 6. The distance of the nuclei of class i to the center nucleus "1" is denoted as r_{1i}.

room temperature (~20 °C). It is driven by a high voltage discharge and generates an acoustic wave whose features evolve as it propagates inside the tank. The pressure signal p_l, characterized with the help of a fibre optic probe hydrophone (FOPH 500, RP.Acoustics) [18] and reported in Fig. 2, exhibits a high pressure front followed by a negative pressure pulse lasting about 4 μs and going down to around -1.4 MPa and then oscillating around zero. The silicon plates are fixed on a thin rod which is coupled to a three axis translation stage (Linos Photonics, x.act LT100 ST). Between two runs the nuclei are ''activated'' (i.e., filled with air). The substrate is first pulled off the water tank, dried by blowing the surface with nitrogen and then immersed in water. If this were not done, the cavitation events of the nuclei would be limited to a few (size-dependent) acoustic cycles [19]. The cavitation events are recorded with a charged coupled device camera (FlowMaster, LaVision) through a long working distance microscope (Model K2, Infinity) lit up with a flash lamp in reflection mode. Only one frame is taken during the overall process and the complete history of the bubble life is scanned by tuning the time interval between the lithotripter and the couple flash camera (Fig. 3). Motion blurring is minimized by a short illumination time of 0.2 μs. We stress here that each data point reported in this Letter corresponds to an individual experiment. The smoothness of the curves in Fig. 4 very convincingly demonstrates the perfect quantitative reproducibility of the cavitation events, i.e., we have achieved controlled surface cavitation.

We have investigated the interaction of bubbles set on a hexagonal lattice with a pitch d equal to 200 μm as depicted in Fig. 1. Because of the geometry, the pattern presents only 6 different classes of cavities. They are numbered by increasing distance from the center and the corresponding number of bubbles in the respective classes 1 to 6 is 1, 6, 6, 6, 12, and 6. A sequence of snapshots

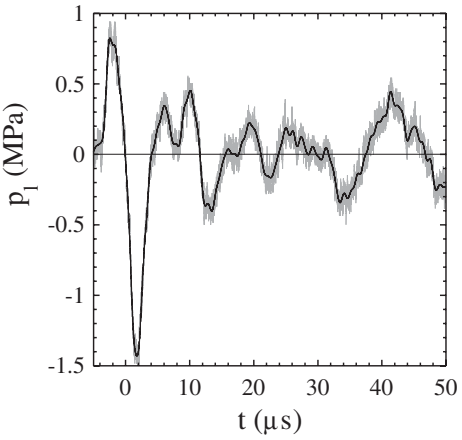

FIG. 2. Pressure generated by the piezoelectric transducer and recorded with a fibre optic probe hydrophone [18]; the dark curve represents the low pass filtered signal. The pressure pulse is used for triggering the expansion of gas pockets trapped on the patterned substrate.

describing the life of the controlled bubble cluster is shown in Fig. 3. The origin of time is chosen to be the time when the bubble at the center starts to grow, corresponding to the arrival of the low pressure part of the wave. The bubbles expand and reach a maximal size after around 10 μs then the bubbles located at the periphery start to collapse triggering the collapse of the inner bubbles. The present symmetry induces an axial focusing flow. Because of the asymmetry introduced by the neighboring bubbles, they form a jet directed towards the center when collapsing [12,20–22]. These jets are particularly visible in the last frame of Fig. 3. Note that the jets are parallel to the wall (due to the interaction with the neighboring bubbles), and not towards the wall as common for the cavitation of bubbles close to a solid boundary [23].

The radius R of the bubbles is deduced from the projected area A measured every 1 μs, i.e., $R = (A/\pi)^{1/2}$. The time evolution of the radius averaged over all individual bubbles within a class (cf. Figure 1) is plotted in Fig. 4. The bubbles in classes 1 and 2 follow a similar trajectory exhibiting a fast expansion phase followed by a plateau and a sudden collapse. This trend is also followed by the bubbles in classes 3 and 4 but with a slightly higher value of the plateau and an earlier collapse of 3 μs. These inner bubbles are shielded by the outer ring formed by bubbles in classes 5 and 6 which grow larger and collapse considerably earlier, as they are more exposed to the surrounding hydrostatic pressure.

Because of the high velocity of the bubble wall during the expansion phase, a few tens of meters per second, the contact line is pinned close to the hydrophobic cavity [24]. A thin liquid film develops below the bubble [25] where the viscous effect are confined. Indeed, the vorticity generated from the wall diffuses on a layer of thickness δ growing with time like $(\nu t)^{1/2}$, where ν is the kinematic viscosity of the water and equal to 10^{-6} m^2/s. The overall cavitation event lasts around 40 μs and thus the viscous effects are confined in a layer close to the wall around 6 μm which is small compared to the bubble size for almost all its lifetime. The liquid is therefore assumed inviscid.

Except during the collapse phase, the contour of the bubbles is circular (Fig. 3). Visualization from the side of an isolated cavity reveals an hemispherical shape [25]. Using the mirror image from the hydrophobic wall we can make an analogy to a two-dimensional cluster evolving in an unbounded domain. The dynamics of the bubbles is thus described by a potential theory giving rise to the well known Rayleigh-Plesset equation for an isolated bubble [1]. Once many nuclei are set close to each other, one has to take into account the interaction between the bubbles through the modification of the pressure field induced by each individual bubble [6]. The advantage of our setup is that the distances r_{ij} between the bubble centers is constant in time and given by the patterning of the substrate (Fig. 1). The radial dynamics $R_i(t)$ of each bubble i is then given by a Rayleigh-Plesset type equation,

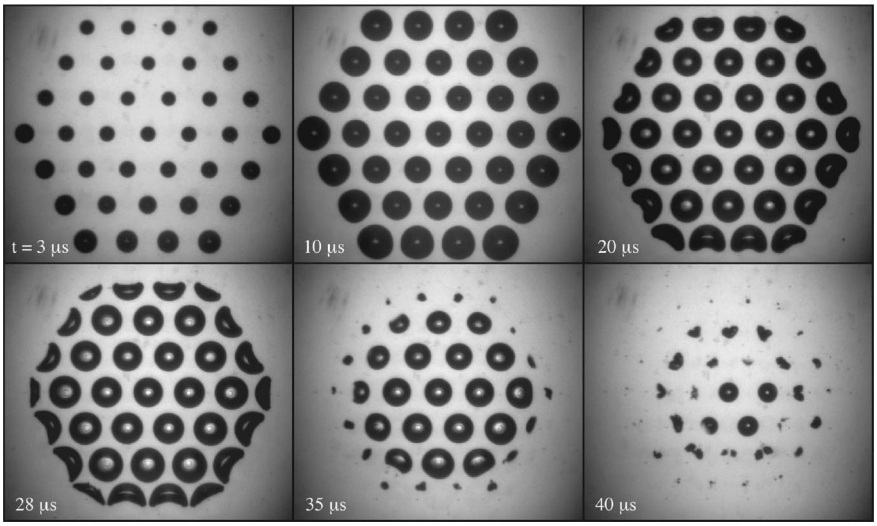

FIG. 3. Time sequence showing the expansion and collapse of a hexagonal cluster of bubbles emerging from a patterned solid surface underwater and triggered by a negative pressure pulse as shown in Fig. 2. The lattice step d is 200 μm. The origin of time is set when the bubble at the center starts to grow. Each snapshot corresponds to an experiment run, the phenomenon being lit by a flash lamp for limiting blurring motion. The slight asymmetry of the bubbles size along the vertical axis in the first picture is due to a nonuniform nucleation time. Indeed, the time needed for the pressure wave traveling from bottom to top (about 1 mm) at the speed of sound (about 1500 m/s) is about 0.7 μs. The initial wall velocity of the bubbles being a few meters per seconds, this delay is enough for inducing this small but visible effect.

$$R_i\ddot{R}_i + \frac{3}{2}\dot{R}_i^2 = \frac{p(R_i) - p_l(t)}{\rho} - \sum_{j\neq i}\frac{R_j^2\ddot{R}_j + 2R_j\dot{R}_j^2}{r_{ij}}, \quad (1)$$

where $p_l(t)$ is the forcing pressure generated by the piezoelectric transducer device (see Fig. 2; in our calculations below we employ the drawn spline fit to the low-path-filtered data). Compressibility effect are not taken into account here as the sound velocity is assumed to be much larger than $\dot{R}_i$. The coupling between the bubbles corresponds to the last term in Eq. (1) and can be seen as the pressure generated by the surrounding bubbles at a distance r_{ij}. The pressure at the bubble wall $p(R_i)$ is related to the inner pressure p_b and the normal constraint induced by the surface tension σ and viscosity η, i.e., $p(R_i) = p_b - \frac{2\sigma}{R_i} - \frac{4\eta}{R_i}\dot{R}_i$. The gas inside the bubble is assumed to follow an isothermal compression linking p_b to the initial bubble size R_0 via a perfect gas law, $p_b = p_v + p_0(R_0/R)^3$, where p_0 is the atmospheric pressure and p_v the vapor pressure. The real radius of curvature of the interface stretched on the cavity is much larger than the cavity diameter and therefore $p_b = p_v + p_0$ at $t = 0$ [26]. The assumption of isothermal

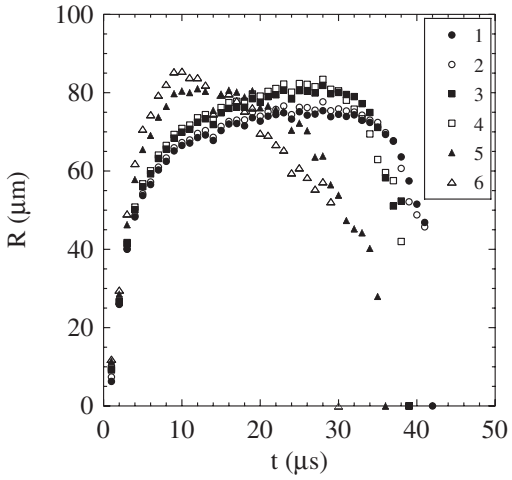

FIG. 4. Time evolutions of the bubble radius for the six spatial locations pointed out in Fig. 1. The size is averaged over all bubbles in the corresponding class. Each data point on one curve has been measured for one experiment, the substrate being removed from the water and dried between successive runs.

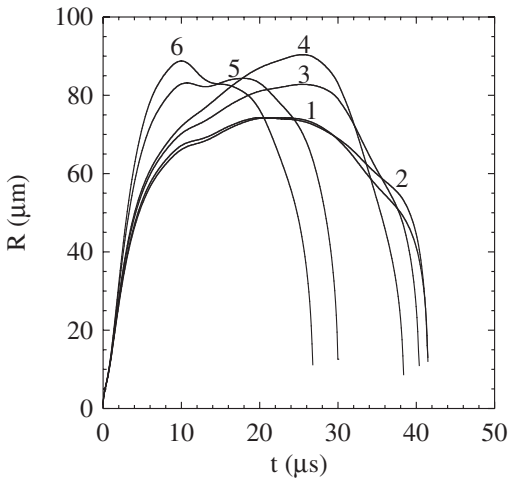

FIG. 5. Bubbles dynamics predicted by a Rayleigh-Plesset approach accounting for bubble-bubble interaction [Eq. (1)] and corresponding to the same conditions as in Fig. 4.

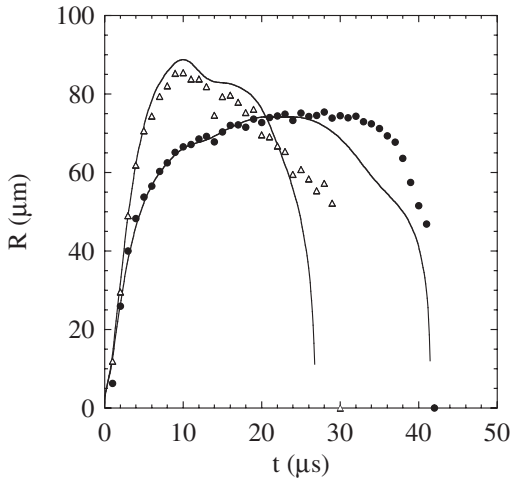

FIG. 6. Comparison between experimental and theoretical evolution of the radius of the bubble at the center ● (class 1) and the most far away △ (class 6).

behavior holds due to the small Peclet number $R\dot{R}/\kappa \ll 1$, apart from at the collapse when the spherical-bubble approximation breaks down anyhow.

The set of six coupled ordinary differential equations (1) is numerically solved. For R_0 we take the radius of a hemisphere having the same volume of the cylindrical cavity etched in the substrate with a diameter D and a depth H, i.e., $R_0 = (3HD^2/8)^{1/3}$. The resulting curves of the radius versus time are plotted in Fig. 5. The maximum size, the lifetime as well as the chronological collapses of the bubbles, seems to be well captured by the model. To further compare with the experiments, the numerical solutions and the measurements of the extreme bubbles, i.e., the number 1 at the center and the number 6 at the edge, are reported together in Fig. 6. An excellent agreement is found except during the collapse phase where the assumption of sphericity is not valid anymore.

In summary, we have introduced a way to control the nucleation of bubbles on a micropatterned solid surface and used it for the study of bubble-bubble interaction in a two-dimensional bubble cluster. The regime of weak interaction, when the bubbles are still hemispherically, can be described by an extended Rayleigh-Plesset type approach, taking the pressure modification through the surrounding bubbles into consideration. It is found that during the cluster collapse the individual bubbles collapse aspherically and they develop a jetting flow directed toward the cluster's center. The natural next step is to study the strong coupling regime, where the bubbles are deformed when getting close to each other and may coalesce. Results on that regime will be reported elsewhere [26].

The authors acknowledge Han Garderniers and his collaborators for microfabrication support. This work is part of the research program of the Stichting voor Fundamenteel Onderzoek der Materie (FOM), which is financially supported by the Nederlandse Organisatie voor Wetenschappelijk Onderzoek (NWO).

*Present address: Ecole Supérieure de Physique et de Chimie Industrielles, 10 rue Vauquelin, 75231 Paris, France.
Email address: Nicolas.Bremond@espci.fr
†Email address: d.lohse@utwente.nl

[1] M. S. Plesset and A. Prosperetti, Annu. Rev. Fluid Mech. **9**, 145 (1977).
[2] C. E. Brennen, *Cavitation and Bubble Dynamics* (Oxford University Press, New York, 1995).
[3] T. G. Leighton, *The Acoustic Bubble* (Academic, London, 1994).
[4] M. P. Brenner, S. Hilgenfeldt, and D. Lohse, Rev. Mod. Phys. **74**, 425 (2002).
[5] E. A. Zabolotskaya, Sov. Phys. Acoust. **30**, 365 (1984).
[6] N. A. Pelekasis, A. Gaki, A. Doinikov, and J. A. Tsamopoulos, J. Fluid Mech. **500**, 313 (2004).
[7] A. A. Doinikov, J. Acoust. Soc. Am. **116**, 821 (2004).
[8] J. R. Blake, G. S. Keen, R. P. Tong, and M. Wilson, Phil. Trans. R. Soc. A **357**, 251 (1999).
[9] C. Wang and B. C. Khoo, J. Comput. Phys. **194**, 451 (2004).
[10] Y. Matsumoto and S. Yoshizawa, Int. J. Numer. Methods Fluids **47**, 591 (2005).
[11] Y. Tomita, A. Shima, and K. Sato, Appl. Phys. Lett. **57**, 234 (1990).
[12] J. R. Blake, P. B. Robinson, A. Shima, and Y. Tomita, J. Fluid Mech. **255**, 707 (1993).
[13] G. E. Reisman, Y. C. Wang, and C. E. Brennen, J. Fluid Mech. **355**, 255 (1998).
[14] N. K. Bourne, Shock Waves **11**, 447 (2002).
[15] S. Granick, Y. Zhu, and H. Lee, Nat. Mater. **2**, 221 (2003).
[16] E. Lauga, M. P. Brenner, and H. A. Stone, in *Handbook of Experimental Fluid Dynamics* (Springer-Verlag, New York, 2006).
[17] T. Dreyer, W. Krauss, E. Bauer, and R. E. Riedlinger, in *Ultrasonics Symposium, San Juan, Puerto Rico: IEEE* (2000), Vol. 2, pp. 1239–1242.
[18] J. Staudenraus and W. Eisenmenger, Ultrasonics **31**, 267 (1993).
[19] N. Bremond, M. Arora, C. D. Ohl, and D. Lohse, J. Phys. Condens. Matter **17**, S3603 (2005).
[20] T. B. Benjamin and A. T. Ellis, Phil. Trans. R. Soc. A **260**, 221 (1966).
[21] J. P. Dear and J. E. Field, J. Fluid Mech. **190**, 409 (1988).
[22] C. D. Ohl and R. Ikink, Phys. Rev. Lett. **90**, 214502 (2003).
[23] A. Philipp and W. Lauterborn, J. Fluid Mech. **361**, 75 (1998).
[24] D. Quéré, Annu. Rev. Fluid Mech. **31**, 347 (1999).
[25] N. Bremond, M. Arora, C. D. Ohl, and D. Lohse, Phys. Fluids **17**, 091111 (2005).
[26] N. Bremond, M. Arora, S. M. Dammer, and D. Lohse (to be published).